

# Faddeev calculations of the $\bar{K}NN$ system with chirally-motivated $\bar{K}N$ interaction.

## I. Low-energy $K^-d$ scattering and antikaonic deuterium.

N.V. Shevchenko<sup>\*1</sup> and J. Révai<sup>2</sup>

<sup>1</sup>*Nuclear Physics Institute, 25068 Řež, Czech Republic*

<sup>2</sup>*Research Institute for Particle and Nuclear Physics,  
H-1525 Budapest, P.O.B. 49, Hungary*

(Dated: April 23, 2018)

### Abstract

A chirally-motivated coupled-channel  $\bar{K}N$  potential, reproducing all low-energy experimental data on  $K^-p$  scattering and kaonic hydrogen and suitable for using in accurate few-body calculations, was constructed. The potential was used for calculations of low-energy amplitudes of the elastic  $K^-d$  scattering using Faddeev-type AGS equations with coupled  $\bar{K}NN$  and  $\pi\Sigma N$  channels. A complex  $K^- - d$  potential reproducing the three-body  $K^-d$  amplitudes was constructed and used for calculation of  $1s$  level shift and width of kaonic deuterium. The predicted shift  $\Delta E_{1s}^{K^-d} \sim -830$  eV and width  $\Gamma_{1s}^{K^-d} \sim 1055$  eV are close to our previous results obtained with phenomenological  $\bar{K}N$  potentials.

PACS numbers: 13.75.Jz, 11.80.Gw, 36.10.Gv

---

\* Corresponding author: shevchenko@ujf.cas.cz

## I. INTRODUCTION

Interaction of antikaon with nucleon is the basis for investigation of atomic and strong quasi-bound states in antikaonic-nucleus systems. Available two-body experimental information on  $\bar{K}N$  interaction is insufficient for construction of a unique interaction model. In particular, it was shown in [1, 2] that phenomenological models of the interaction having one or two poles for the  $\Lambda(1405)$  resonance reproducing all low-energy experimental data on  $K^-p$  scattering and kaonic hydrogen equally well can be constructed. A way to obtain some additional information about the  $\bar{K}N$  interaction is to use it as an input in an accurate few-body calculation and then compare the theoretical predictions with eventual experimental data.

There are several calculations devoted to the low-energy  $K^-d$  scattering [3, 4] or the  $K^-d$  scattering length only [5, 6] based on Faddeev equations. Low-energy  $K^-d$  amplitudes, including scattering length, and effective range were calculated in our papers [1, 2]. In the most recent one [2] the directly measurable characteristics of  $1s$  level of kaonic deuterium were calculated as well. It allows the direct comparison of the theoretical predictions with eventual experimental data on kaonic deuterium, which hopefully will be obtained in SIDDHARTA-2 experiment [7].

The results were obtained by solving coupled-channel Faddeev-type AGS equations with phenomenological  $\bar{K}N$  potentials. However, many other authors of  $\bar{K}N$  interaction models use not a phenomenological, but a chirally-motivated potential, where a  $\bar{K}N$  amplitude obtained from a chiral Lagrangian is used as a potential to determine the position of the poles of  $\Lambda(1405)$  resonance. Bethe-Salpeter or Lippmann-Schwinger equations are used for this task. There are quite a few such chirally-motivated potentials available, however, none of them is suited for use in Faddeev calculations since either they have too many coupled channels and cannot be used as it is or they are not as accurate in reproducing experimental data as one would wish. Therefore, we decided to construct a new chirally-motivated model of  $\bar{K}N$  interaction, which can be used in dynamically accurate three-body calculations.

The potential reproduces the low-energy data on  $K^-p$  scattering and kaonic hydrogen with the same level of accuracy as our previously constructed phenomenological  $\bar{K}N$  potentials. We repeated our calculation of the low-energy  $K^-d$  elastic scattering and the characteristics of kaonic deuterium using the new model of  $\bar{K}N$  interaction and compared

the new results with those obtained using phenomenological  $\bar{K}N$  potentials. Since the three-body AGS equations and the rest of the two-body input are the same in both calculations, we could isolate the pure effect of the different types of  $\bar{K}N$  interaction models.

The description of the chirally motivated potential is given in the next section, the results on the low-energy  $K^-d$  scattering are given and discussed in Sec. III. Sec. IV contains information on the evaluation of kaonic deuterium  $1s$  level shift and width, while Sec. V concludes the paper.

## II. CHIRALLY-MOTIVATED $\bar{K}N - \pi\Sigma - \pi\Lambda$ POTENTIAL

There are many different chirally-motivated models of  $\bar{K}N$  interaction in the literature [8–10]. Most of them are not really suited for use in Faddeev calculations since they have too many coupled channels. Recently, one more of these  $\bar{K}N$  potentials was constructed [11] together with a reduced version, which contains only three channels. Therefore, this last one, in principle, could be used in a dynamically correct few-body calculation, however, the reduced version does not reproduce  $K^-p$  experimental data accurately enough.

The commonly used  $s$ -wave chirally-motivated potentials have the energy-dependent part (see e.g. [9])

$$\bar{V}^{ab}(\sqrt{s}) = \sqrt{\frac{M_a}{2\omega_a E_a}} \frac{C^{ab}(\sqrt{s})}{(2\pi)^3 f_a f_b} \sqrt{\frac{M_b}{2\omega_b E_b}} \quad (1)$$

and are written in particle basis. We took into account all open particle channels:  $a, b = K^-p, \bar{K}^0n, \pi^+\Sigma^-, \pi^0\Sigma^0, \pi^-\Sigma^+$  and  $\pi^0\Lambda$ . Baryon mass  $M_a$ , baryon energy  $E_a$  and meson energy  $w_a$  of the channel  $a$  enter the factors, which ensure proper normalization of the amplitude. The non-relativistic form of the leading order Weinberg-Tomozawa interaction

$$C^{ab}(\sqrt{s}) = -C^{WT} (2\sqrt{s} - M_a - M_b) \quad (2)$$

was used with SU(3) Clebsh-Gordan coefficients  $C_I^{WT}$ .

Our chirally motivated potential  $V_{\bar{K}N}^{Chiral}$  is separable, it contains also form-factors and is written in isospin basis:

$$V_{II'}^{\alpha\beta}(k^\alpha, k'^\beta; \sqrt{s}) = g_I^\alpha(k^\alpha) \bar{V}_{II'}^{\alpha\beta}(\sqrt{s}) g_{I'}^\beta(k'^\beta), \quad (3)$$

where  $V_{II'}^{\alpha\beta}(\sqrt{s})$  is the energy-dependent part of the potential in isospin basis, obtained from Eq.(1). The  $k^\alpha, k'^\alpha$  and  $\sqrt{s}$  stand for the initial, final relative momenta and the total energy,

TABLE I: Parameters of the chirally-motivated  $V_{\bar{K}N-\pi\Sigma-\pi\Lambda}^{Chiral}$  potential: the pseudo-scalar meson decay constants  $f_\pi, f_K$  (MeV) and the range parameters  $\beta_I^\alpha$  ( $\text{fm}^{-1}$ ).

$f_\pi$	$f_K$	$\beta_0^{\bar{K}N}$	$\beta_0^{\pi\Sigma}$	$\beta_1^{\bar{K}N}$	$\beta_1^{\pi\Sigma}$	$\beta_1^{\pi\Lambda}$
116.20	113.36	4.06	3.30	5.00	3.86	1.99

respectively. We used physical masses in the calculations, therefore the two-body isospin  $I = 0$  or  $1$  is not conserved. Yamaguchi form-factors

$$g_I^\alpha(k^\alpha) = \frac{(\beta_I^\alpha)^2}{(k^\alpha)^2 + (\beta_I^\alpha)^2} \quad (4)$$

were used in Eq.(3). The channel indices  $\alpha, \beta$  take three values denoting the  $\bar{K}N$ ,  $\pi\Sigma$  and  $\pi\Lambda$  channels.

The pseudo-scalar meson decay constants  $f_\pi, f_K$  and the range parameters  $\beta_I^\alpha$ , depending on the two-body isospin, are free parameters, which were found by fitting the potential to the experimental data. In the same way as the phenomenological ones, the potential (3) reproduces elastic and inelastic  $K^-p$  cross-sections, threshold branching ratios  $\gamma, R_c, R_n$  and characteristics of  $1s$  level of kaonic hydrogen. The parameters of the potential are shown in Table I.

All physical observables to be compared with experimental data were obtained from solution of the Lippmann-Schwinger equation with the potential  $V_{\bar{K}N}^{Chiral}$  (3) and Coulomb interaction since, as previously, we wanted to calculate characteristics of kaonic hydrogen directly, without intermediate reference to  $K^-p$  scattering length. We used non-relativistic kinematics while the potential was constructed. Among all authors of  $\bar{K}N$  potentials only we and Cieply, Smejkal [9, 12] take Coulomb interaction into account directly when calculating the  $1s$  level shift and width of kaonic hydrogen. All other calculations of the same quantity get it from the  $K^-p$  scattering length through the approximate ‘‘corrected Deser’’ formula [13]. However, as it was shown in [12, 14] the approximate formula gives 10% error, therefore the direct calculation of the  $1s$  level shift and width of kaonic hydrogen is desirable.

The observables given by the potential are shown in Table II together with the corresponding experimental data. It is seen that the  $1s$  level shift  $\Delta E_{1s}^{K^-p}$  and width  $\Gamma_{1s}^{K^-p}$  of

TABLE II: Physical characteristics of the chirally motivated  $V_{\bar{K}N-\pi\Sigma-\pi\Lambda}^{Chiral}$  potential:  $1s$  level shift  $\Delta E_{1s}^{K^-p}$  (eV) and width  $\Gamma_{1s}^{K^-p}$  (eV) of kaonic hydrogen, threshold branching ratios  $\gamma$ ,  $R_c$  and  $R_n$  together with experimental data. The experimental data on kaonic hydrogen are those obtained by SIDDHARTA collaboration.

	$V_{\bar{K}N-\pi\Sigma-\pi\Lambda}^{Chiral}$	Experiment
$\Delta E_{1s}^{K^-p}$	-313	$-283 \pm 36 \pm 6$ [21]
$\Gamma_{1s}^{K^-p}$	561	$541 \pm 89 \pm 22$ [21]
$\gamma$	2.35	$2.36 \pm 0.04$ [22, 23]
$R_c$	0.663	$0.664 \pm 0.011$ [22, 23]
$R_n$	0.191	$0.189 \pm 0.015$ [22, 23]

kaonic hydrogen of the  $V_{\bar{K}N}^{Chiral}$  are in agreement with the most recent experimental data of SIDDHARTA collaboration [21]. Comparing the data in Table II with those from Table 2 of [2] we see that the chirally motivated potential  $V_{\bar{K}N}^{Chiral}$  gives  $1s$  level shift  $\Delta E_{1s}^{K^-p}$  and width  $\Gamma_{1s}^{K^-p}$  of kaonic hydrogen, which is close to the results of the one-pole  $V_{\bar{K}N-\pi\Sigma}^{1,SIDD}$  and the two-pole  $V_{\bar{K}N-\pi\Sigma}^{2,SIDD}$  versions of the phenomenological potential. The chirally motivated potential also reproduces the rather accurately measured threshold branching ratios  $\gamma$ ,  $R_c$  and  $R_n$ :

$$\gamma = \frac{\Gamma(K^-p \rightarrow \pi^+\Sigma^-)}{\Gamma(K^-p \rightarrow \pi^-\Sigma^+)}, \quad (5)$$

$$R_c = \frac{\Gamma(K^-p \rightarrow \pi^+\Sigma^-, \pi^-\Sigma^+)}{\Gamma(K^-p \rightarrow \text{all inelastic channels})}, \quad (6)$$

$$R_n = \frac{\Gamma(K^-p \rightarrow \pi^0\Lambda)}{\Gamma(K^-p \rightarrow \text{neutral states})}. \quad (7)$$

The medium value of the threshold branching ratio  $\gamma$  and of the  $R_{\pi\Sigma}$  constructed from the  $R_c$  and  $R_n$  (see Eqs.(7,10) of [2]) are reproduced by the phenomenological potential as well, therefore, we can say that all three potentials reproduce the experimental data equally well.

The same is true for the elastic and inelastic  $K^-p$  cross-sections  $K^-p \rightarrow K^-p$ ,  $K^-p \rightarrow \bar{K}^0n$ ,  $K^-p \rightarrow \pi^+\Sigma^-$ ,  $K^-p \rightarrow \pi^-\Sigma^+$ , and  $K^-p \rightarrow \pi^0\Sigma^0$ . In order to demonstrate, that all three potentials reproduce the cross-sections with the same accuracy, we plotted the results of  $V_{\bar{K}N}^{Chiral}$ ,  $V_{\bar{K}N-\pi\Sigma}^{1,SIDD}$  and  $V_{\bar{K}N-\pi\Sigma}^{2,SIDD}$  model of interaction in the same figure, see Figure 1. The

experimental data in the figure are taken from [15–19]. As previously, one set of data [20] is neglected due to large experimental errors.

Unlike most of the authors of models of  $\bar{K}N$  interaction we need not know  $K^-p$  scattering length  $a_{K^-p}$  to calculate the characteristics of kaonic hydrogen. However, we can calculate it directly from the  $V_{\bar{K}N}^{Chiral}$  potential, its value is

$$a_{K^-p} = -0.77 + i 0.84 \text{ fm}. \quad (8)$$

The isospin zero and one  $\bar{K}N$  scattering lengths

$$a_{\bar{K}N,0} = -1.65 + i 1.26 \text{ fm}, \quad a_{\bar{K}N,1} = 0.52 + i 0.48 \text{ fm} \quad (9)$$

are not connected with the  $a_{K^-p}$  value by a simple formula since physical masses are used while the  $V_{\bar{K}N}^{Chiral}$  is constructed together with isospin nonconserving Coulomb interaction. Put in three-body AGS equations, however, isospin averaged masses are used, which lead to different values of the scattering lengths:

$$a_{K^-p}^{aver} = -0.49 + i 0.71 \text{ fm}, \quad (10)$$

$$a_{\bar{K}N,0}^{aver} = -1.50 + i 0.84 \text{ fm}, \quad a_{\bar{K}N,1}^{aver} = 0.53 + i 0.59 \text{ fm}. \quad (11)$$

In the same way as other chirally-motivated potentials, our new potential has two strong poles for the  $\Lambda(1405)$  resonance:

$$z_1 = 1417 - i 33 \text{ MeV}, \quad z_2 = 1406 - i 89 \text{ MeV}. \quad (12)$$

Both are situated on the proper Riemann sheets, corresponding to a resonance in  $\pi\Sigma$  channel and a quasi-bound state in  $\bar{K}N$  channel. They are connected to  $\pi\Lambda$  channel too through isospin nonconserving parts. The real parts of the poles are situated between the  $\bar{K}N$  and  $\pi\Sigma$  thresholds as one would expect. The two-pole structure of the  $\Lambda(1405)$  resonance follows from the energy-dependent form of the potential. To achieve the same property of our two-pole phenomenological potential  $V_{\bar{K}N-\pi\Sigma}^{2,SIDD}$  we used a more complicated form-factor in the  $\pi\Sigma$  channel.

In the same way as in [14] we checked, where the poles move when the nondiagonal couplings of the potential were gradually reduced to zero. The results are demonstrated in Fig. 2. It is seen, that the strong pole  $z_1$  becomes a real bound state with smaller than the original binding energy when the  $\bar{K}N$ ,  $\pi\Sigma$  and  $\pi\Lambda$  channels are uncoupled. The second

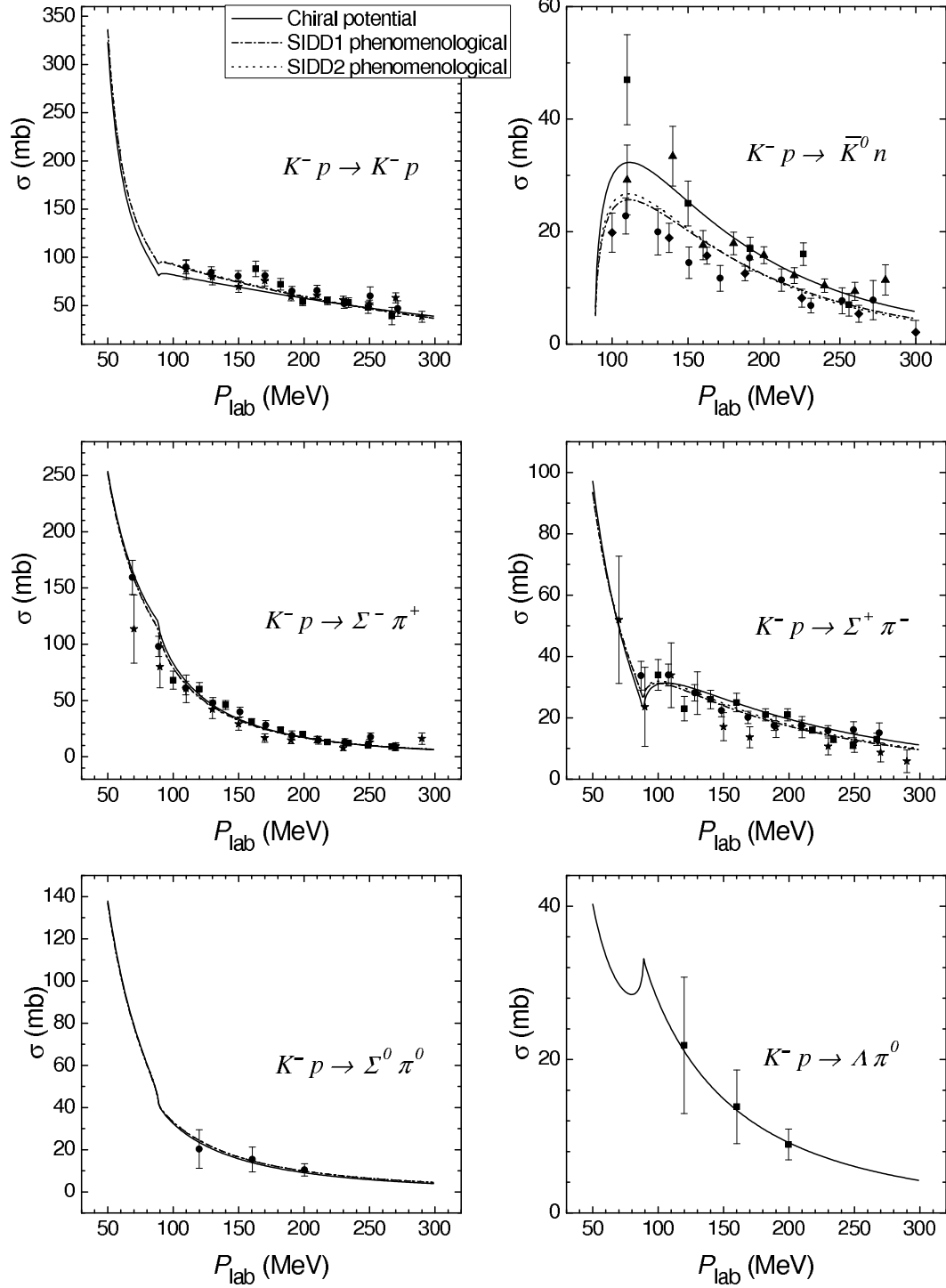


FIG. 1: Comparison of the elastic and inelastic  $K^- p$  cross-sections for the chirally motivated potential  $V_{\bar{K}N}^{\text{Chiral}}$  (solid lines) with the one-pole  $V_{\bar{K}N-\pi\Sigma}^{1,\text{SIDD}}$  (dash-dotted lines) and two-pole  $V_{\bar{K}N-\pi\Sigma}^{1,\text{SIDD}}$  (dotted lines) phenomenological potentials from [2]. The experimental data are taken from [15–19] (data points).

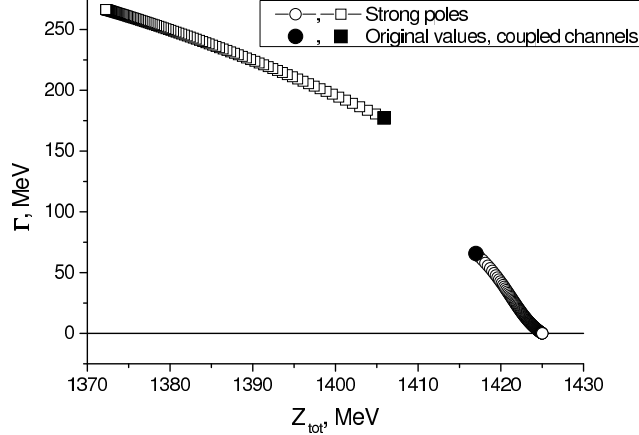


FIG. 2: Trajectories of the strong poles when the coupling between the  $\bar{K}N$ ,  $\pi\Sigma$  and  $\pi\Lambda$  channels is gradually being switched off (empty symbols). The filled symbols denote the original values with coupled channels.

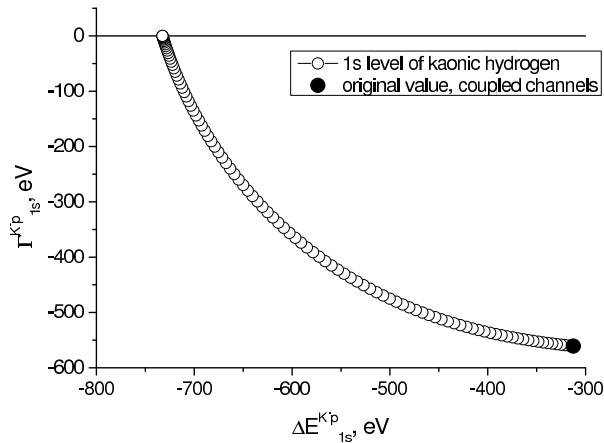


FIG. 3: The same as Fig. 2 for the 1s level of kaonic hydrogen.

strong pole  $z_2$  remains a resonance pole, situated between the  $\bar{K}N$  and  $\pi\Sigma$  channels, but with smaller real and larger imaginary parts. The same trajectory drawn for the 1s level shift and width of kaonic hydrogen, see Fig. 3, shows that the pole, corresponding to the atomic state, also becomes a real bound state. The 1s level shift is large for the decoupled system.

Theoretically, the  $\Lambda(1405)$  resonance peak could be seen in the elastic  $\pi^0\Sigma^0$  cross-sections, however, the corresponding experimental peak can be observed only as an FSI peak in a more complicated reaction involving three or more particles. In this case the virtual  $\bar{K}N \rightarrow \pi\Sigma$  process can also contribute to the  $\pi\Sigma$  yield in a final state. The extent of this contribution can be reliably determined only by considering the complete, rather complicated

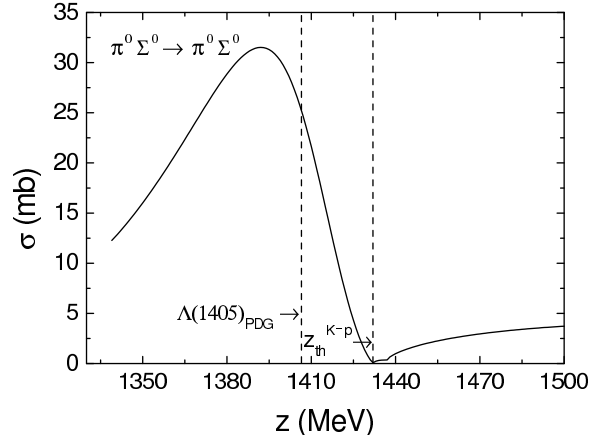


FIG. 4: Elastic  $\pi^0\Sigma^0$  cross-sections of the chirally motivated potential  $V_{\bar{K}N}^{Chiral}$ . The PDG value for the mass of  $\Lambda(1405)$  resonance and the  $K^-p$  threshold are also shown.

process (see e.g. Eq.(11) in [24]). Instead, many authors of  $\bar{K}N$  interaction models add the  $\bar{K}N \rightarrow \pi\Sigma$  amplitude to the  $\pi\Sigma \rightarrow \pi\Sigma$  one and introduce an adjustable parameter in front of it to compare the theoretical predictions with experimental  $\pi\Sigma$  missing mass spectra. The corresponding cross-sections are multiplied by  $\pi\Sigma$  relative momentum, which is a phase space factor coming from the FSI formalism. We did not follow that routine and demonstrate the effect of  $\Lambda(1405)$  resonance in elastic  $\pi^0\Sigma^0$  cross-sections, see Figure 4.

### III. $K^-d$ ELASTIC SCATTERING AND $K^-d$ QUASI-BOUND STATE

We solved Faddeev-type equations in Alt-Grassberger-Sandhas form for the  $\bar{K}NN$  system with coupled  $\pi\Sigma N$  channel, the formulas can be found in our previous paper [1]. The equations properly describe three-body dynamics of the system. They are written in momentum representation, isospin formalism is used. The equations were properly antisymmetrised, which is necessary due to two baryons in every channel. The logarithmic singularities in the kernels of the equations were treated by the method suggested in [25]. The three-body calculations were performed without taking Coulomb interaction into account since the effect of it is expected to be small.

The elastic  $K^-d$  amplitudes, including the scattering length, and effective range were calculated using the chirally-motivated  $V_{\bar{K}N-\pi\Sigma-\pi\Lambda}^{Chiral}$  potential described in the previous section. We used averaged masses in the potential as well as in the the whole three-body calculation since it was shown in [24] that the effect of physical masses is rather small. The three-channel

$\bar{K}N - \pi\Sigma - \pi\Lambda$  potential was used in the  $\bar{K}NN - \pi\Sigma N$  AGS equations in a form of the exact optical two-channel  $\bar{K}N - \pi\Sigma(-\pi\Lambda)$  potential, when the  $\bar{K}N - \bar{K}N$ ,  $\bar{K}N - \pi\Sigma$  and  $\pi\Sigma - \pi\Sigma$  elements of the three-channel  $T$ -matrix are used as the two-channel  $T$ -matrix. The remaining two-body potentials, needed for the three-body calculation, are also separable. The two-term TSA-B  $NN$  and the exact optical  $\Sigma N(-\Lambda N)$  potentials, which were used, are described in [1]. The  $NN$  model of interaction reproduces phase shifts of Argonne V18 potential, therefore, is repulsive at short distances. It gives proper  $NN$  scattering length, effective range and binding energy of deuteron. The two-channel  $\Sigma N - \Lambda N$  potential reproduces experimental  $\Sigma N$  and  $\Lambda N$  cross-sections, the corresponding exact optical  $\Sigma N(-\Lambda N)$  potential has exactly the same elastic  $\Sigma N$  amplitude as the two-channel potential.

The  $K^-d$  scattering length  $a_{K^-d}$  obtained with the chirally-motivated potential is shown in Table III. The new three-body result is compared to those from [2] with one-  $V_{\bar{K}N-\pi\Sigma}^{1,SIDD}$  and two-pole  $V_{\bar{K}N-\pi\Sigma}^{2,SIDD}$  versions of phenomenological  $\bar{K}N$  potential. The ‘‘phenomenological’’ results in the Table slightly differ from the three-body values from Table 2 of [2] since here we used the spin-independent  $\Sigma N(-\Lambda N)$  potential, while the spin-dependent was used in the previous paper. It is seen, that the chirally motivated potential leads to about 6% larger absolute value of the real and the imaginary part of the scattering length. The difference is quite small, so we can conclude, that the three different models of  $\bar{K}N$  interaction, which reproduce low-energy data on  $K^-p$  scattering and kaonic hydrogen with the same level of accuracy, give quite similar results for low-energy  $K^-d$  scattering.

Since it was shown [1] that Fixed Scatterer Approximation, also called Fixed Center Approximation, gives very large error for the  $K^-d$  system, this time we do not compare the results obtained with this method with ours. Four  $a_{K^-d}$  values obtained in other Faddeev calculations are shown in Table III. Comparing to them, we see that the result of the very recent calculation with coupled channels [6] gives real part of  $a_{K^-d}$ , which almost coincides with our result for chirally motivated potential. The imaginary part of the  $K^-d$  scattering length from [6] is slightly larger, which can follow from the fact that the model of  $\bar{K}N$  interaction used there was fitted to kaonic hydrogen data not directly, but through the  $K^-p$  scattering length and the approximate formula, which is the least reliable just in reproducing the imaginary part of the level shift.

The one-channel result of Faddeev calculation [5] lies far away from all the others. Two effects play their role here: a one-channel dynamics and, therefore, indirect taking  $\pi\Sigma N$

TABLE III: Scattering lengths of  $K^-d$  scattering  $a_{K^-d}$  (fm) and effective range  $r_{K^-d}^{eff}$  (fm) obtained from AGS calculations with the chirally-motivated  $V_{\bar{K}N-\pi\Sigma-\pi\Lambda}^{Chiral}$  potential (3) and the one-pole  $V_{\bar{K}N-\pi\Sigma}^{1,SIDD}$  and two-pole  $V_{\bar{K}N-\pi\Sigma}^{2,SIDD}$  phenomenological potentials from [2].  $K^-d$  scattering length values from other Faddeev calculations are also shown.  $1s$  level shift  $\Delta E_{1s}^{K^-d}$  (eV) and width  $\Gamma_{1s}^{K^-d}$  (eV) of kaonic deuterium, calculated using the three potentials, are shown as well.

	$a_{K^-d}$	$r_{K^-d}^{eff}$	$\Delta E_{1s}^{K^-d}$	$\Gamma_{1s}^{K^-d}$
AGS with $V_{\bar{K}N}^{Chiral}$ , this work	$-1.59 + i 1.32$	$0.50 - i 1.17$	-828	1055
AGS with $V_{\bar{K}N}^{1,SIDD}$ , [2]	$-1.49 + i 1.24$	$0.69 - i 1.31$	-785	1018
AGS with $V_{\bar{K}N}^{2,SIDD}$ , [2]	$-1.51 + i 1.25$	$0.69 - i 1.34$	-797	1025
MFST, [6]	$-1.58 + i 1.37$			
Deloff, [5]	$-0.85 + i 1.05$			
TDD, [4]	$-1.34 + i 1.04$			
TGE, [3]	$-1.47 + i 1.08$			

channel into account and problems with reproducing experimental data by the complex  $\bar{K}N$  potential. It was demonstrated in [1] for phenomenological models of  $\bar{K}N$  interaction that simple complex potentials have quite large error, while an exact optical  $\bar{K}N$  potential gives rather accurate result for the scattering length. The exact optical potential with  $\bar{K}N$  amplitudes exactly corresponding to those from the potential with coupled channels is good for the chirally motivated model as well. It gives

$$a_{K^-d}^{Chiral,Opt} = -1.57 + i 1.32 \text{ fm}, \quad (13)$$

which is very close to the coupled-channel result from Table III.

Finally, two old  $a_{K^-d}$  values [3, 4] significantly underestimate the imaginary part of the  $K^-d$  scattering length.

We also calculated effective range  $r_{K^-d}^{eff}$  of  $K^-d$  scattering, the results can be seen in Table III. The real part of  $r_{K^-d}^{eff}$  of the chirally motivated potential is much smaller than those of our phenomenological potentials. The imaginary part is smaller by the absolute value. The near-threshold elastic amplitudes of  $K^-d$  scattering are needed for construction of

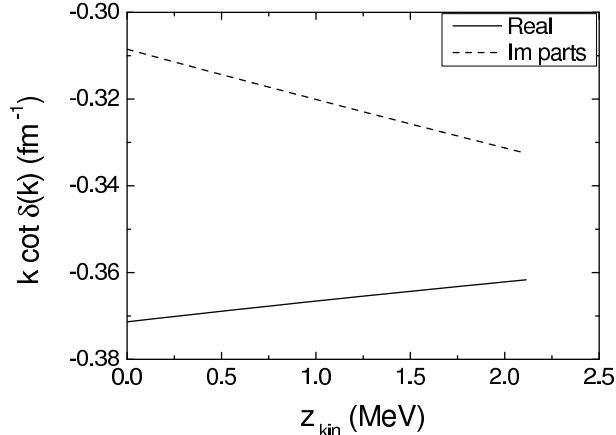


FIG. 5: Real (solid line) and imaginary (dashed line) parts of the elastic near-threshold  $K^-d$  amplitudes presented in a form of  $k \cot \delta(k)$  function. The results were obtained from the coupled-channel three-body AGS equations using the chirally motivated potential  $V_{\bar{K}N}^{\text{Chiral}}$ .

a complex two-body  $K^- - d$  potential and further calculation of  $1s$  level of kaonic deuterium. They are presented in  $k \cot \delta(k)$  form in Figure 5.

The relative values of  $|\text{Re } a_{K^-d}|$  and  $|\text{Im } a_{K^-d}|$  obtained with all three our potentials together with their signs might lead to the conclusion that a bound or a quasi-bound state could exist in the  $K^-d$  system. However, this conclusion is not true. We solved an eigenvalue problem using the same AGS equations and found that such a state does not exist. Details of the calculations can be found in our next paper, devoted to the quasi-bound state in  $K^-pp$  system. The reason why the estimation is not reliable is that it is based on the effective range expansion of a scattering amplitude. The expansion allows to derive simple relations between a scattering length and a bound state of a system, however, its validity is limited to the vicinity of the corresponding threshold. Since the  $K^-d$  state is expected to have rather large width, it is definitely out of such a region. The only  $\bar{K}N$  potential, which gives a quasi-bound state in  $K^-d$  system, is one of our older phenomenological potentials [1], which does not reproduce SIDDHARTA, but KEK data on kaonic hydrogen [26] only.

#### IV. CHARACTERISTICS OF KAONIC DEUTERIUM

Our aim was to calculate a physical quantity, which characterizes low-energy properties of  $K^-d$  system and can be compared to experimental data directly. The scattering length is not of this type, while the  $1s$  level shift and width of kaonic deuterium can be measured.

Therefore, we calculated these atomic observables, which correspond to the results of our three-body calculations of low-energy  $K^-d$  scattering.

Since Faddeev calculation with Coulomb plus strong interaction is too hard, a two-body calculation with a complex  $K^- - d$  potential was performed instead. The potential is a separable one with two terms

$$V_{K^-d}(\vec{k}, \vec{k}') = \lambda_{1,K^-d} g_1(\vec{k}) g_1(\vec{k}') + \lambda_{2,K^-d} g_2(\vec{k}) g_2(\vec{k}') \quad (14)$$

and Yamaguchi form-factors

$$g_i(k) = \frac{1}{\beta_{i,K^-d}^2 + k^2}, \quad i = 1, 2. \quad (15)$$

The parameters of the potential

$$\beta_{1,K^-d} = 1.5 \text{ fm}^{-1}, \quad \lambda_{1,K^-d} = -0.0628 - i 0.4974 \text{ fm}^{-2} \quad (16)$$

$$\beta_{2,K^-d} = 1.1, \text{ fm}^{-1}, \quad \lambda_{2,K^-d} = -0.1123 + i 0.1556 \text{ fm}^{-2} \quad (17)$$

were fixed by fitting the three-body  $K^-d$  amplitudes calculated using the AGS equations, described in the previous section. Obviously, the potential (14) reproduces the scattering length  $a_{K^-d}$  and effective range  $r_{K^-d}^{eff}$  from Table III.

The Lippmann-Schwinger equation with the complex  $K^- - d$  and Coulomb potentials was then solved and the  $1s$  level energy was obtained. More details about the calculation can be found in [2]. The shift  $\Delta E_{1s}^{K^-d}$  and width  $\Gamma_{1s}^{K^-d}$  of kaonic deuterium, corresponding to the chirally motivated model of  $\bar{K}N - \pi\Sigma - \pi\Lambda$  interaction are shown in Table III. We also show the characteristics of the atom, obtained with our phenomenological potentials  $V_{\bar{K}N-\pi\Sigma}^{1,SIDD}$  and  $V_{\bar{K}N-\pi\Sigma}^{2,SIDD}$  [2].

The ‘‘chirally motivated’’ absolute values of the level shift  $\Delta E_{1s}^{K^-d}$  and the width  $\Gamma_{1s}^{K^-d}$  are both larger than those obtained in [2] for the phenomenological  $\bar{K}N - \pi\Sigma$  potentials. Keeping in mind the results for the  $K^-d$  scattering lengths discussed in the previous section it is an expected result since the  $1s$  level shift and width of an hadronic atom are directly connected to the strong scattering length of the system. However, the results obtained using three different models of  $\bar{K}N$  interaction are rather close to each other. We think, that the important point here is the fact that all three potentials reproduce low-energy experimental data on  $K^-p$  scattering and kaonic hydrogen with the same level of accuracy.

We checked the accuracy of the approximate corrected Deser formula, allowing simple computation of characteristics of a kaonic atom from a known scattering length. The result obtained using the  $a_{K^-d}$  value from Table III:

$$\Delta E_{K^-d,cD}^{Chiral} = -878 \text{ eV}, \quad \Gamma_{K^-d,cD}^{Chiral} = 724 \text{ eV}, \quad (18)$$

compared to more accurate ones  $\Delta E_{K^-d}^{Chiral}$ ,  $\Gamma_{K^-d}^{Chiral}$  from the same Table show that in this case the error of the approximate formula is as large as for the case of phenomenological  $\bar{K}N$  potentials. As in [2], the corrected Deser formula underestimates the width of the  $1s$  level of kaonic deuterium by 30%. Therefore, the validity of this statement does not depend on the model of the  $\bar{K}N$  interaction.

We would like to note that our results for the  $\Delta E_{K^-d}^{Chiral}$  and  $\Gamma_{K^-d}^{Chiral}$ , shown in Table III can not be called “exact”, but only “accurate” since the  $1s$  level shift and width were obtained from the two-body calculation with a point-like deuteron, interacting with a kaon through the complex potential. It means that the size of deuteron was taken into account only effectively through the potential, which reproduces the three-body  $K^-d$  AGS amplitudes. As for the corrected Deser formula, it contains no three-body information at all since the only input is a  $K^-d$  scattering length. Moreover, the formula relies on further approximations, which are absent in our calculation, and give a 10% error already for the two-body case.

## V. CONCLUSIONS

We constructed three-channel isospin dependent chirally-motivated  $\bar{K}N - \pi\Sigma - \pi\Lambda$  potential and used it in the Faddeev-type calculations of the low-energy elastic  $K^-d$  amplitudes, including  $K^-d$  scattering length, and effective range. The potential reproduces all low-energy experimental data on  $K^-p$  scattering and characteristics of kaonic hydrogen with the same level of accuracy as our phenomenological potentials with one- and two-pole structure of  $\Lambda(1405)$  resonance. Comparison of the results allows to reveal the effect of the three different models of  $\bar{K}N$  interaction used in the three-body calculations. It turns out that low-energy  $K^-d$  elastic amplitudes and characteristics of kaonic deuterium obtained with the three potentials are rather close. Therefore, comparison with eventual results of an experiment on kaonic deuterium hardly could choose one of the models of  $\bar{K}N$  interaction. Additionally, we found no quasi-bound states in the  $K^-d$  system.

**Acknowledgments.** The work was supported by the Czech GACR grant P203/12/2126 and the Hungarian OTKA grant 109462. One of the authors (NVS) is thankful to J. Haidenbauer for his comments on some details of  $\bar{K}N$  models of interaction.

---

- [1] N.V. Shevchenko, Phys. Rev. C 85, 034001 (2012).
- [2] N.V. Shevchenko, Nucl. Phys. A 890-891, 50 (2012).
- [3] G. Toker, A. Gal, J.M. Eisenberg, Nucl. Phys. A 362, 405 (1981).
- [4] M. Torres, R.H. Dalitz, A. Deloff, Phys. Lett. B 174, 213 (1986).
- [5] A. Deloff, Phys. Rev. C 61, 024004 (2000).
- [6] T. Mizutani, C. Fayard, B. Saghai, K. Tsushima, Phys. Rev. C 87, 035201 (2013).
- [7] C. Curceanu *et al.*, Nucl. Phys. A 914, 251 (2013).
- [8] B. Borasoy, U.-G. Meißner, R. Niffler, Phys. Rev. C **74**, 055201 (2006).
- [9] A. Cieplý, J. Smejkal, Nucl. Phys. A 881, 115 (2012).
- [10] Z.-H. Guo, J.A. Oller, Phys.Rev. C 87, 035202 (2013).
- [11] Y. Ikeda, T. Hyodo, W. Weise, Nucl.Phys. A 881, 98 (2012).
- [12] A. Cieplý, J. Smejkal, Eur. Phys. J A 34, 237 (2007).
- [13] U.-G. Meißner, U. Raha, A. Rusetsky, Eur. Phys. J. C 35, 349 (2004).
- [14] J. Révai, N.V. Shevchenko, Phys. Rev. C 79, 035202 (2009).
- [15] M. Sakitt *et al.*, Phys. Rev. 139, B719 (1965).
- [16] J.K. Kim, Phys. Rev. Lett. 14, 29 (1965); Phys. Rev. Lett. 19, 1074 (1967).
- [17] W. Kittel, G. Otter, and I. Wacek, Phys. Lett. 21, 349 (1966).
- [18] J. Ciborowski *et al.*, J. Phys. G 8, 13 (1982).
- [19] D. Evans *et al.*, J. Phys. G 9, 885 (1983).
- [20] W.E. Humphrey, R.R. Ross, Phys. Rev. 127, 1305 (1962).
- [21] M. Bazzi *et al.* (SIDDHARTA Collaboration), Phys. Lett. B 704, 113 (2011).
- [22] D.N. Tovee *et al.*, Nucl. Phys. B 33, 493 (1971).
- [23] R.J. Nowak *et al.*, Nucl. Phys. B 139, 61 (1978).
- [24] J. Révai, Few-Body Syst. 54, 1865 (2013).
- [25] F. Sohre and H. Ziegelman, Phys. Lett. B 34, 579 (1971).
- [26] T.M. Ito *et al.*, Phys. Rev. C 58, 2366 (1998).